Heliyon 10 (2024) e39564

Contents lists available at ScienceDirect

Heliyon

journal homepage: www.cell.com/heliyon

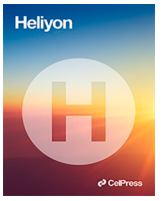

Research article

Sophora alopecuroide - Taraxacum decoction (STD) inhibits non-small cell lung cancer via inducing ferroptosis and modulating tumor immune microenvironment

Ouyang Xiaohu [a,1], Jingbo Wang [a,1], Xiaoyuan Qiu [a], Shuxin Song [a], Junyi Li [a], Shanshan Luo [b], Qianyun Chen [a,**], Desheng Hu [a,c,*]

[a] *Department of Integrated Traditional Chinese and Western Medicine, Union Hospital, Tongji Medical College, Huazhong University of Science and Technology, Wuhan, 430022, China*

[b] *Institute of Hematology, Union Hospital, Tongji Medical College, Huazhong University of Science and Technology, Wuhan, 430022, China*

[c] *China-Russia Medical Research Center for Stress Immunology, Union Hospital, Tongji Medical College, Huazhong University of Science and Technology, Wuhan, 430022, China*

ARTICLE INFO

Keywords:
Sophora alopecuroide
Taraxacum decoction
Ferroptosis
Tumor immune microenvironment
Non-small cell lung cancer

ABSTRACT

The Sophora alopecuroide - Taraxacum Decoction (STD) is a traditional Chinese herbal formulation that has demonstrated significant potential in combating tumors. Despite its apparent effectiveness, the specific mechanisms through which STD exerts its anti-tumor properties remain largely unexplored and are yet to be fully understood. In our study, we provided evidence that STD effectively inhibits cellular growth and movement, as well as halting the cell cycle at the G2/M checkpoint. Furthermore, our pharmacological network analysis indicated that STD might induce cell death through a process known as ferroptosis. This hypothesis was substantiated by observing important biochemical changes associated with ferroptosis, including a decrease in glutathione (GSH) levels, an increase in iron accumulation, and elevated levels of reactive oxygen species (ROS) and lipid peroxidation. Additionally, we noted a significant rise in the expression of pro-ferroptosis genes such as Keap1, Nrf2, and HO-1, further supporting our findings. Significantly, and in line with the *in vitro* results, STD also showed a strong ability to inhibit tumor growth by inducing ferroptosis in a subcutaneous tumor model. Additionally, STD treatment changed the tumor immune microenvironment (TIME), as seen by an increase in $CD107a^{+}$ CD8 and NK cells within the tumor. These findings demonstrate that STD induces ferroptosis and alters TIME to combat tumors, suggesting that STD may be a viable alternative treatment for patients with NSCLC.

Abbreviations: STD, Sophora alopecuroide - Taraxacum decoction; NSCLC, non-small cell lung cancer; TIME, tumor immune microenvironment; TFRC, Transferrin receptor-1; ROS, reactive oxygen species; GSH, Glutathione; SLC7A11, Solute carrier family 7 member 11; TCM, traditional Chinese medicine; SAL, *Sophora alopecuroides* Linn; TCMSP, Traditional Chinese Medicine System Pharmacology Database and Analysis Platform; KEGG, Kyoto Encyclopedia of Genes and Genomes.

* Corresponding author. Department of Integrated Traditional Chinese and Western Medicine, Union Hospital, Tongji Medical College, Huazhong University of Science and Technology, Wuhan, 430022, China.

** Corresponding author.

E-mail addresses: 511958685@qq.com (Q. Chen), desheng.hu@hust.edu.cn (D. Hu).

[1] These authors contributed equally to this study.

https://doi.org/10.1016/j.heliyon.2024.e39564
Received 20 April 2024; Received in revised form 4 October 2024; Accepted 17 October 2024
Available online 19 October 2024

1. Introduction

Lung cancer remains the second leading cause of cancer mortality worldwide, accounting for more fatalities than the combined totals of colorectal, breast, and prostate cancers [1,2]. The majority of lung cancer cases were non-small cell lung cancer (NSCLC), which remains one of the most aggressive and malignant tumor types, despite significant advancements being made in standard NSCLC treatments, including surgery, chemotherapy, radiotherapy, targeted therapy, and immunotherapy [3]. Therefore, it is crucial to provide a different, efficient treatment or medication with minimal adverse effects for NSCLC.

Induction of tumor cell death is the fundamental mechanism by which current therapies treat cancer. Ferroptosis, a novel form of programmed cell death originally identified in 2012, was typified by the iron-dependent accumulation of polyunsaturated fatty acid peroxides [4]. Ferroptosis's morphological characteristics, including reduced mitochondrial size, heightened membrane density, and the absence of clearly marked mitochondrial cristae, were primarily observed in mitochondria. Large membrane blebs were also frequently found in ferroptosis [5]. Two pathways are the main regulators of ferroptosis. The extrinsic route is initiated by the activation of lactotransferrin and serotransferrin, two iron transporters, or by the inhibition of cell membrane transporters such the cystine/glutamate transporter. Ferroptosis is intrinsically initiated when intracellular antioxidant enzymes are inhibited [6]. Transferrin receptor-1 (TFRC)-mediated iron uptake promotes ferroptosis, whereas SLC40A1-mediated iron export inhibits it [7,8]. Ferritin, an iron storage protein complex composed of FTH1 and FTL, prevents Fe^{2+} from being oxidized by reactive oxygen species (ROS) [9]. Glutathione (GSH) is a crucial antioxidant [10]. The solute carrier family 7 member 11 (SLC7A11) and GPX4, both essential proteins for the synthesis and utilization of GSH, are also closely associated with ferroptosis [11]. Additionally, ACSL3 aids cancer cells in resisting ferroptosis by suppressing lipid peroxidation in the cell membrane [12]. The Nrf2/HMOX1 pathway has frequently been implicated in the induction of ferroptosis in tumor cells [13–15]. HO-1 activity catalyzes the oxidative cleavage of heme at the α-methene bridge carbon, generating equivalent amounts of carbon monoxide (CO) and biliverdin (BV), while releasing the central heme iron chelate as Fe^{2+}, thereby initiating the ferroptosis process [16]. Ferroptosis plays a crucial regulatory role in the occurrence and progression of several diseases, including neurodegenerative diseases, acute kidney injury, hepatic disease, gastrointestinal and pancreatic disorders, and particularly cancer [17]. Cancer cells are more susceptible to ferroptosis than normal cells due to their higher iron requirements for rapid cell cycles [18]. Inducing ferroptosis presents a potential strategy for cancer treatment and overcoming drug resistance. However, the rapidly growing yet still disorganized body of knowledge regarding the molecular mechanisms and structural requirements of ferroptosis-inducing agents hampers current drug development, despite the belief that this approach holds promise for treating aggressive, metastatic, and therapy-resistant cancers [19].

Traditional Chinese medicine (TCM), one of the most significant complementary therapies globally, has demonstrated promise in the prevention and treatment of lung cancer. Numerous studies have investigated the use of TCM decoctions in treating non-small cell lung cancer (NSCLC) through the mechanism of ferroptosis. Fuzheng Kang'ai decoction primarily promotes ferroptosis in NSCLC by inhibiting GPX4 expression [20]. Alantolactone induced ferroptosis by enhancing intracellular Fe^{2+} buildup through enhancing FTH1 degradation [21]. Agrimonolide inhibits the aggressive growth of NSCLC and encourages ferroptosis by blocking the mTOR signaling pathway [22]. Auriculasin disrupts the PI3K/Akt pathway in NSCLC, promoting mitochondrial oxidative stress and ferroptosis [23]. Additional research indicates that TCM can impede the spread of lung cancer by modifying the tumor immune microenvironment (TIME). The Yangyinwenyang formula stimulates mature dendritic cells, facilitating the priming of T cells into T helper 1 cells or cytotoxic T cells [24]. Another decoction, Yu-Ping-Feng, prevents lung cancer metastasis by enhancing the cytotoxicity of $CD4^+$ T cells and promoting M1 macrophage polarization [25]. The combination of Taraxacum and Sophora alopecuroide, referred to as Sophora alopecuroide - Taraxacum Decoction (STD), is derived from the 'Handbook of Xinjiang Herbal Medicine', a contemporary herbal medicine reference published by the Xinjiang Army Logistics Department's Ministry of Health. In China's Uyghur gathering area, KPD has frequently been employed to treat lung cancer, although the underlying mechanisms remain largely unclear. The total flavonoids of Taraxacum mongolicum inhibit NSCLC progression by promoting tumor cell apoptosis and enhancing the cytotoxic activity of $CD8^+$ T lymphocytes [26]. Furthermore, taraxasterol, one of the active compounds in Taraxacum, exhibits potent anticancer effects by inducing tumor cell apoptosis and increasing $CD107a^+$ NK cells in NSCLC [27]. Quinolizidine alkaloids, significant active components isolated from Sophora alopecuroides Linn (SAL), have demonstrated an antitumor effect on NSCLC by enhancing PD-L1 expression, thereby improving the efficacy of PD-L1 blockade therapy through the ADORA1-ATF3 axis [28]. However, the precise mechanism underlying the combination of Taraxacum and Sophora alopecuroides in the treatment of NSCLC remains unclear.

This investigation established that STD exhibits anticancer properties against NSCLC. Subsequently, we employed network pharmacology analysis to predict the potential role of STD in NSCLC treatment. Our findings indicated that the primary mechanisms underlying STD's anticancer effects include the induction of ferroptosis and regulation of the tumor immune microenvironment (TIME). Therefore, these results offer new insights for future NSCLC treatment strategies.

2. Materials and methods

2.1. Preparation of Sophora alopecuroide - Taraxacum decoction (STD)

Sophora alopecuroide - Taraxacum Decoction (STD) is a mixture of two herbs including *Sophora alopecuroides* (Ku Dou Zi) (5 g) and *Taraxacum mongolicum* (Pu Gong Ying) (15 g). The herbs were purchased from Min-Nong-Ren (Dingxi, Gansu, China) and were identified by two professional herbalists. The herbs were first soaked in purified water for three times to remove impurities. *Sophora alopecuroides* was first boiled in 1000 ml water with strong heat for 1 h to obtain the aqueous extraction. Then *Taraxacum mongolicum*

was added and boiled together with gentle heat for additional 1 h. Then freeze-dried power of decoction was obtained via a rotary evaporator. Subsequently, the freeze-dried power was directly stored, or was dissolved into a 20 mg/ml concentration with DMEM medium and filtered with 0.22 μm filter membrane and stored at −80 °C for long-term use.

2.2. Component analysis of STD powder with UPLC-MS/MS

The freeze-dried powder was dissolved in 70 % methanol, and kept at −20 °C for 4 h. After centrifugation at 20,000 g for 15 min at 4 °C, the solution was run through a 0.22 μm filter for preparing LC-MS analysis. The sample extracts were then analyzed by using UPLC (Waters, USA) with QTRAP 6500 Plus (SCIEX, USA). The samples were injected into the ACQUITY UPLC®HSS T3 column (100*2.1 mm, 1.8 μm, Waters) and eluted for MRM monitoring with the following LC gradient: 95 % mobile phase A (Waters with 0.1% FA) and 5 % mobile phase B (Acetone with 0.1%FA) at 10 min to 5 % mobile phase A and 95 % mobile phase B at 22 min with the flow rate of 0.3 mL/min, the column temperature was set at 40 °C. The following source parameters were specified for the QTRAP 6500 Plus outfitted with an EST Turbo Ion-Spray interface: Ion source gas I (GS1), gas II (GS 2), and curtain gas (CUR) were set at 40, 40, and 20 psi, respectively. Source temperature: 500 °C. Ion spray voltage: 4500 V (positive mode) or −4500 V (negative mode). Target metabolite retention duration, MRM transitions, collision energy (CE), declustering potential energy (DP), and scheduling mode were all configured for MRM procedures.

2.3. Cell lines, cell culture and siRNA transfection

The Department of Respiratory and Critical Care Medicine at Wuhan Union Hospital in China contributed human NSCLC cell lines (H1299, A549) as well as mouse NSCLC cell lines (Lewis lung carcinoma, LLC). LLC cells were cultivated in Dulbecco's modified Eagle's medium (DMEM) (Gibco, United States) with 10 % fetal bovine serum (FBS); H1299 and A549 cells were cultured at Roswell Park Memorial Institute (RPMI)-1640 (Gibco, United States) with 10 % FBS. Cells were incubated at 37 °C in a humidified environment containing 5 % CO2. siRNA was transfected with 3000proMax per manufacturer's instructions (OBiO Technology, Shanghai, China). To test the efficiency of siRNA-mediated knockdown of protein of interest, total proteins of transfected cells were extracted at 24 h post-transfection and were analyzed by qPCR and Western blotting assay.

2.4. CCK-8 assay

Cell proliferation was determined using the cell counting kit-8 test (CCK-8, GK10001, GlpBio, USA). In 96-well plates, 3×10^3 LLC, H1299, or A549 cells were planted and exposed to STD at different dosages for 24 h, 48 h, and 72 h, respectively. Following the procedure, the CCK-8 reagent was added to the cells, which were then incubated for an additional 1 h at 37 °C. The absorbance was measured at 450 nm with a microplate reader (Molecular Devices, San Jose, California, USA).

2.5. 5-Ethynyl-2-deoxyuridine (EdU) assay

The proliferation capacity of LLC, H1299, and A549 cells were measured using a Cell Proliferation Edu Image Kit (Abbkine, Wuhan, China). The nuclei were stained with 4',6-diamidino-2-phenylindole (DAPI, Abbkine) to mark the cells in wells. The fluorescent pictures were imaged and recorded under a fluorescence microscope (Olympus Corporation, Japan).

2.6. Cell cycle assay

A propidium iodide (PI) Cell Cycle Staining Kit (Multi Sciences Biotech, Zhejiang, China) was used to measure the cell cycle. LLC, H1299, and A549 cells were obtained after being incubated with STD at different concentrations for 24 h. Following this, the cells were twice washed in phosphate buffer saline (PBS) that had been precooled, and then they were stained with permeabilization and DNA staining solutions at room temperature (RT) for half an hour in the dark. Following washing, the cells were sent to flow cytometry (CytoFLEX, Backman Counter, Brea, CA, USA) for counting and examination. CytExpert 2.4 software was then used to evaluate the results.

2.7. Wound healing assay

When the cells cover the bottom of the 6-well plate, they were scraped with a sterile plastic tip for the wound healing assay. The cells grow in a serum-free media supplemented with STD at various doses and incubated at 37 °C for 24 h. The wound was examined under a microscope (CX53, Olympus-life science, Tokyo, Japan) after being cleansed twice with PBS.

2.8. Colony formation assays

LLC, H1299, and A549 cells are grown in 6 cm dishes for 24 h before to being exposed to STD at different concentrations for a week in order to perform the colony formation assay. After that, the cells were fixed for 10 min at RT using 4 % paraformaldehyde (Servicebio, Wuhan, China), twice-washed in PBS, and stained for 20 min using 0.1 % crystal violet (G1014, Servicrbio, China). To facilitate study, the number of colonies was counted.

2.9. Corresponding target intersection of STD

The potential targets of the active compounds in STD were screened from TCMSP database (https://old.tcmsp-e.com/tcmsp). And the target of NSCLC were obtained from 5 databases, namely, GeneCards (https://www.genecards.org/), OMIM (https://www.omim.org/), PharmGkb (https://www.pharmgkb.org/), Therapeutic Target Database (https://db.idrblab.net/ttd/), and DrugBank (https://go.drugbank.com/).

2.10. Gene ontology (GO) pathway enrichment analysis

There are 143 genes in total that are associated with lung cancer and STD. Then, the GO function enrichment of those targets retrieved from databases were performed using the R language and the "clusterProfiler", "enrichplot", and "ggplot2" packages. The only terms that were deemed significantly enriched had a p-value and q-value of 0.05 or lower.

2.11. Assay of GSH

A GSH assay kit (A006-2-1) from Jiancheng (Nanjing, China) was used to determine total GSH. In short, 2×10^5 cells per well of 6-well plates were used to cultivate LLC, H1299, and A549 cells. After the cells were incubated with the STD for 24 h, they were collected, resuspended in PBS, and sonicated to lyse them. After centrifugation, the supernatant was gathered to measure the GSH content.

Table 1
Primer sequence of RT-qPCR.

Species	Gene	Primer sequence (5′–3′)
Human	β-actin	TCGTGCGTGACATTAAGGAG
		ATGCCAGGGTACATGGTGGT
Human	Keap1	CAACTTCGCTGAGCAGATTGGC
		TGATGAGGGTCACCAGTTGGCA
Human	Nrf2	CACATCCAGTCAGAAACCAGTGG
		GGAATGTCTGCGCCAAAAGCTG
Human	HIF1A	TATGAGCCAGAAGAACTTTTAGGC
		CACCTCTTTTGGCAAGCATCCTG
Human	HMOX1	CCAGGCAGAGAATGCTGAGTTC
		AAGACTGGGCTCTCCTTGTTGC
Human	SLC7A11	TCCTGCTTTGGCTCCATGAACG
		AGAGGAGTGTGCTTGCGGACAT
Human	SLC40A1	GAGACAAGTCCTGAATCTGTGCC
		TTCTTGCAGCAACTGTGTCACAG
Human	GPX4	ACAAGAACGGCTGCGTGGTGAA
		GCCACACACTTGTGGAGCTAGA
Human	ACSL3	CTTTCTCACGGATGCCGCATTG
		CTGCTGCCATCAGTGTTGGTTTC
Human	FTL	TACGAGCGTCTCCTGAAGATGC
		GGTTCAGCTTTTTCTCCAGGGC
Human	HSP90AA1	TCTGCCTCTGGTGATGAGATGG
		CGTTCCACAAAGGCTGAGTTAGC
Human	FTH1	TGAAGCTGCAGAACCAACGAGG
		GCACACTCCATTGCATTCAGCC
Mouse	β-actin	CATTGCTGACAGGATGCAGAAGG
		TGCTGGAAGGTGGACAGTGAGG
Mouse	Keap1	ATCCAGAGAGGAATGAGTGGCG
		TCAACTGGTCCTGCCCATCGTA
Mouse	Nrf2	CAGCATAGAGCAGGACATGGAG
		GAACAGCGGTAGTATCAGCCAG
Mouse	HMOX1	CACTCTGGAGATGACACCTGAG
		GTGTTCCTCTGTCAGCATCACC
Mouse	HIF1A	CCTGCACTGAATCAAGAGGTTGC
		CCATCAGAAGGACTTGCTGGCT
Mouse	SLC7A11	CTTTGTTGCCCTCTCCTGCTTC
		CAGAGGAGTGTGCTTGTGGACA
Mouse	SLC40A1	CCATAGTCTCTGTCAGCCTGCT
		CTTGCAGCAACTGTGTCACCGT
Mouse	GPX4	CCTCTGCTGCAAGAGCCTCCC
		CTTATCCAGGCAGACCATGTGC
Mouse	ACSL3	GCGAGAAGGATTCCAAGACTGG
		GAAGAGTAGCCGATTCGGCATC
Mouse	FTL	CCTCGAGTTTCAGAACGATCGC
		CCTGATTCAGGTTCTTCTCCATG

2.12. Intracellular iron measurement

Using an iron colorimetric test kit (E-BC-K880-M, Elabscience, Wuhan), total intracellular irons were detected. In 6-well plates, LLC, H1299, and A549 cells were cultivated at a density of 2×10^5 cells per well. After receiving STD treatment for 24 h, cells were harvested and lysed. The amount of irons was measured after centrifuging the supernatant.

2.13. Measurement of ROS

LLC, H1299, and A549 cells were treated as indicated and incubated with fresh medium containing 10 mM DCFH-DA (Beyotime Biotechnology, China) at 37 °C for 30 min. The cells were then washed with PBS for 3 times. After that, a BECKMAN COULTER flow cytometer was used to gauge the amount of ROS presence in the treated cells.

2.14. Measurement of lipid ROS

Lipid peroxidation senso (BODIPY™ 581/591C11, D3861, Invitrogen, USA) was used to measure the levels of lipid ROS. LLC, H1299, and A549 cells were grown in 6-well plates with a density of 2×10^5 cells per well. Cells were gently rinsed with PBS after being incubated with STD for 24 h, and then they were incubated with BODIPY™ 581/591C11 (10 μM) for 30 min at 37 °C. A flow cytometer (BECKMAN COULTER) was used to assess the amount of lipid ROS.

2.15. Quantitative real-time PCR analysis

The cells were first cultivated for 24 h while exposed to various STD doses. To extract total RNA, cell pellets were processed with the RNAiso plus (9109, TaKaRa, Japan) reagent. Using the SynScript III cDNA Synthesis Mix kit from Tsingke Biotechnology Beijing, China, total RNA was reverse-transcribed into cDNA. Then, real-time PCR was carried out using an ABI 7300 Real-Time PCR apparatus and the AceQ qPCR SYBR Green MasterMix (Q111-02/03, Vazyme, Nanjing). The final data was then analyzed using the 2ˆ(−△△CT) method after a dissolution curve had been created. The internal reference was β-actin. The primer sequences are displayed in Table 1.

2.16. Western blot analysis

After STD therapy, cells and subcutaneous xenograft tumor samples were lysed to extract total protein using RIPA lysate (G2002, Servicebio, Wuhan, China). Protein samples were placed onto sodium dodecyl sulfate-polyacrylamide gel electrophoresis (SDS-PAGE) gels at 10 %, 12 %, or 15 % before being transferred to a PVDF membrane with a thickness of 0.22 μm. After blocking in TBST with 5 % skim milk at RT for 1.5 h on a shaker, the PVDF membrane was incubated with the appropriate primary antibodies for an overnight incubation at 4 °C. Following 10-min TBST rinses for three times, the PVDF membrane was placed in the secondary antibody incubation solution for 1 h at RT. The membranes were imaged using an imaging system (iBright 750, Invitrogen, USA) following incubation with the ELC reagent (a mixture of solutions A and B in equal proportion) (Biosharp, Hefei, China). By using Image J software, protein levels were calculated.

2.17. Immunofluorescence

Cells were sown in 24-well plates and grown for 24 h prior to immunofluorescence microscopy. Additionally, after draining the medium, cells were permeabilized with 0.5 % Triton X-100 in PBS for 15 min after being fixed with 4 % paraformaldehyde for 15 min, and then washed with PBS for three times with 5 min each. Then, 3 % BSA in PBS was used to further block cells for 30 min. The cells were then rinsed with PBS for three times with 5 min each after being incubated with the primary antibody anti-HMOX1 (1:100) (catalog number A1346; Abclonal, Wuhan, Chian; dilution, 1:1000) all night long at 4 °C. The cells were then treated with fluorescently tagged secondary antibodies (catalog number AS007; Abclonal, Wuhan, China; dilution, 1:100) for 45 min at RT before being washed with PBS for three times with 5 min each. Then pre-warmed ER-Green staining (KeyGEN BioTECH, Jiangsu, China) working solution was added at 37 °C and incubate with the cells for 15–30 min at 37 °C. The nuclei were marked with DAPI. Finally, a fluorescence microscope of Olympus was used to find fluorescently labeled target proteins.

2.18. In vivo tumor model

All the *in vivo* experimental protocols were approved by the animal Nursing Committee of Tongji Medical College of the Huazhong University of Science and Technology. Male C57BL/6J mice with six weeks old were bought from Rat Laibao Biotechnology in Wuhan, China. The mice were adaptive fed for seven days. After that, they were subcutaneously injected with 100 μL of medium containing 8×10^5 LLC cells. After five days, the mice were randomly assigned to three groups: the high dose group, the low dose group, and the control group. Every two days, the mice's weights were measured and the tumor volume was computed using the formula (short diameter) 2 × (long diameter)/2. Twelve days after daily gavage therapy was administered, the mice were killed by cervical dislocation, and the tumor tissue was extracted for imaging and recording.

2.19. Flow cytometry analysis

Single cell suspensions were obtained as previously described [29]. FVD was used to determine the alive and dead cells, and then antibodies specific for CD45, CD4, CD8, NK1.1, F4/80, CD11c, CD107a, and CD11b, were used to stain the surface markers on cells. For intracellular staining, cells were then stained intracellularly using an intracellular staining kit (554714, BD Biosciences) for the detection of CD206, T-bet, RORγt and Foxp3. The Beckman Coulter CytoFLEX was used for flow cytometry, and CytExpert 2.4 software was used to interpret the results.

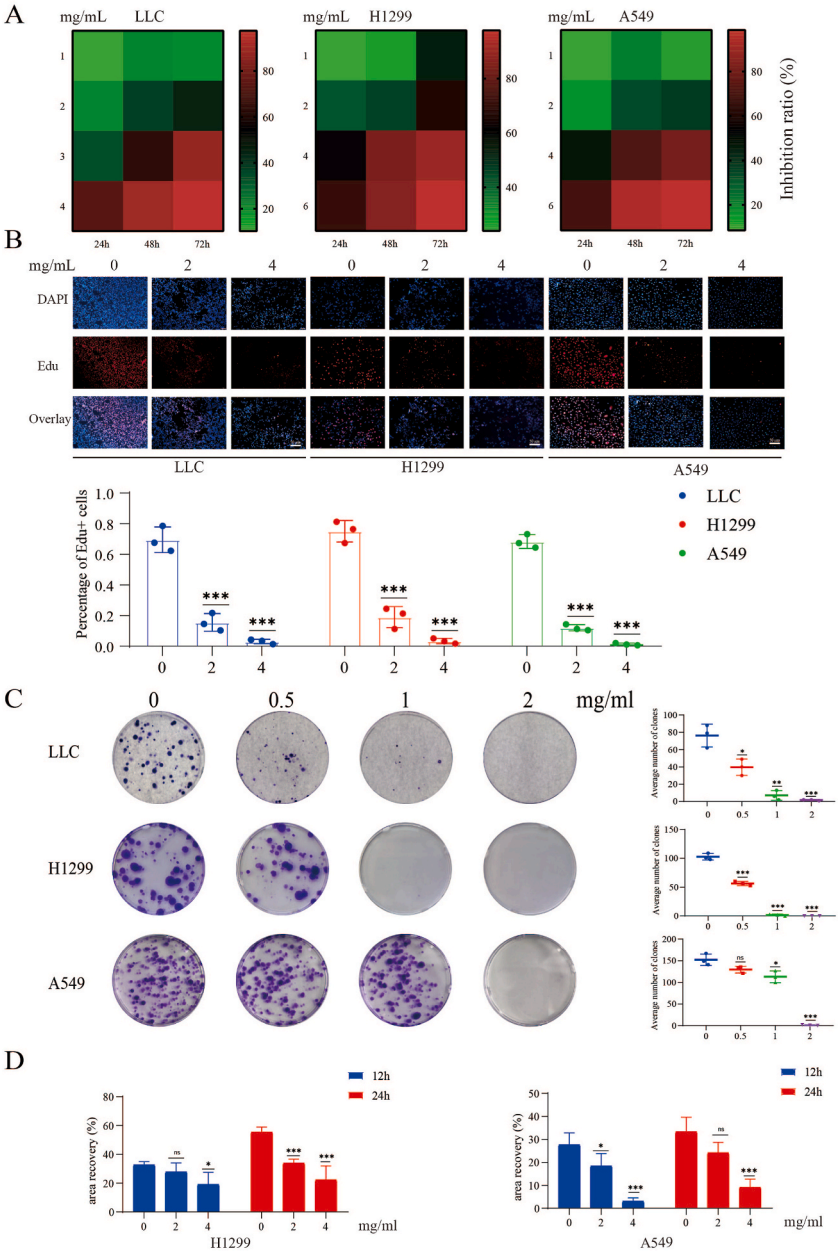

Fig. 1. Multiparameter screening of STD with high cytotoxicity properties. (A) The CCK-8 assays were used to compare the drug's cytotoxicity to NSCLC cells at the relevant dosages and time points. As a measure of cell viability, the inhibition ratio was determined using the average O.D. values for each condition (n = 5). (B) 5-ethynyl-2' -deoxyuridine (Edu) assay was used to measure cell proliferation. (C) Crystal violet staining was performed to demonstrate the colony-formation ability, and cell counting was performed using Image J software. (D) Representative results of wound healing assays in NSCLC cells following a 24 h treatment with STD.

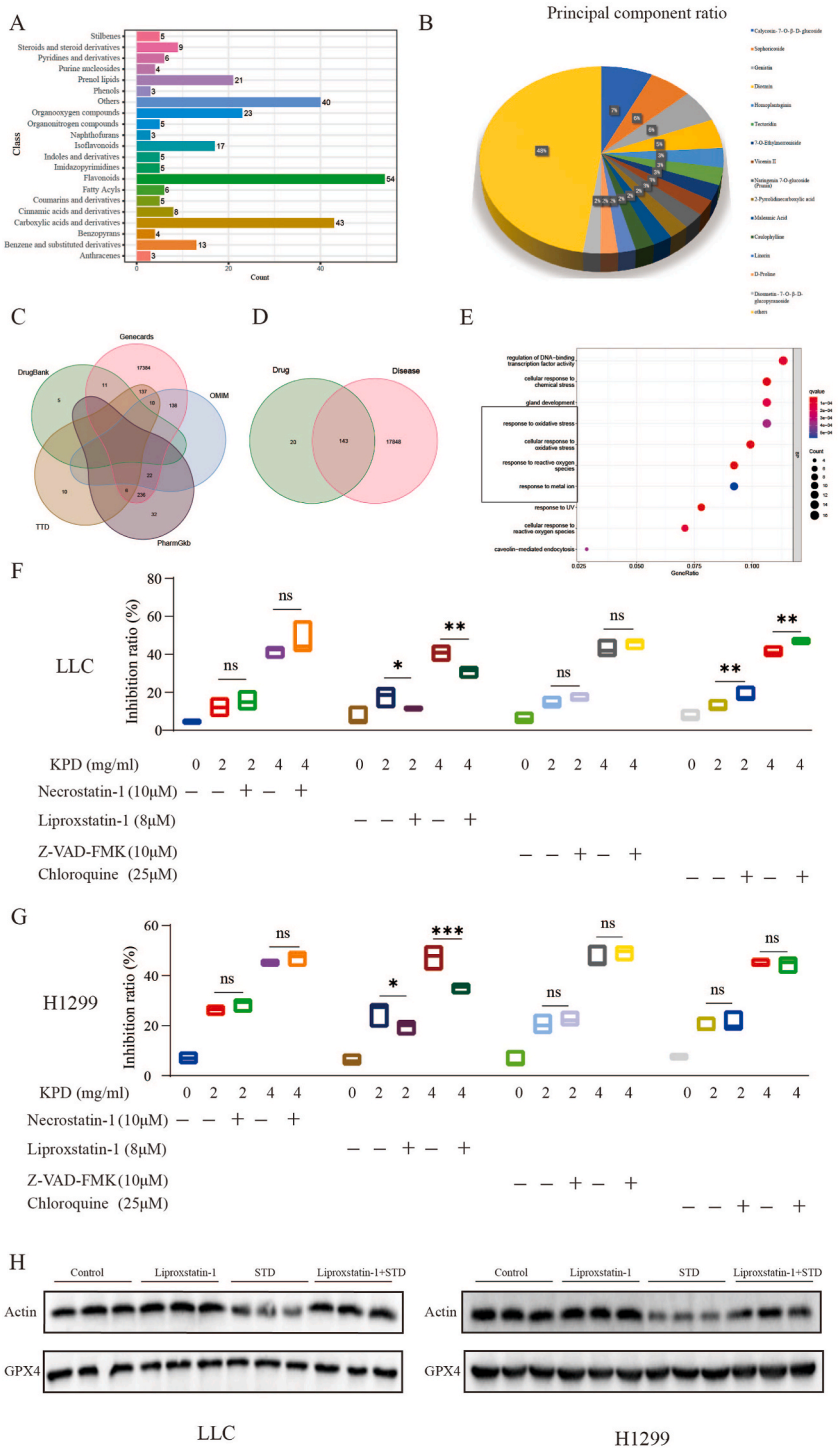

Fig. 2. The network pharmacology analysis and verification of STD. (A–B) LC-MS analysis was applied to identified the main components in STD decoction. (C–D) Potential targets for STD in the treatment of lung cancer. (E) GO analysis reveals the possible functions of STD. (F–G) LLC, and H1299 cells were cotreated with STD with or without Z-VAD-FMK, Necrostatin-1, Liproxstatin-1 and Chloroquine for 24 h, and cell vitality was assayed by the CCK-8 assay. (H) The expression of GPX4 protein in LLC and H1299 cells treated with STD, Liproxstatin-1, and the two combined.

2.20. Serum BUN, Cre, ALT and AST detection mice

Mice's peripheral venous blood was gathered, and centrifugation (3000 rpm for 10 min) was used to separate the serum. The levels of serum BUN, Cre, ALT and AST were assessed following the protocols outlined in the reagent kits from Nanjing Jiancheng Bioengineering Institute, located in Nanjing, China.

2.21. Clinical characteristics of ferroptosis-related genes

The "ggplot2", "limma", "ggpubr", and "Survival" R packages were applied to investigate the connection between target genes expression and the clinical characteristics of LUAD patients.

2.22. Statistical analysis

GraphPad Prism version 8 software was used to analyze and create graphs for all data, which were all presented as mean ± standard deviation (SD). ANOVA or the Student's *t*-test was used to evaluate group differences. P values below 0.05 were regarded as significant indicators. And the following p values were labeled: *p < 0.05; **p < 0.01; ***p < 0.001.

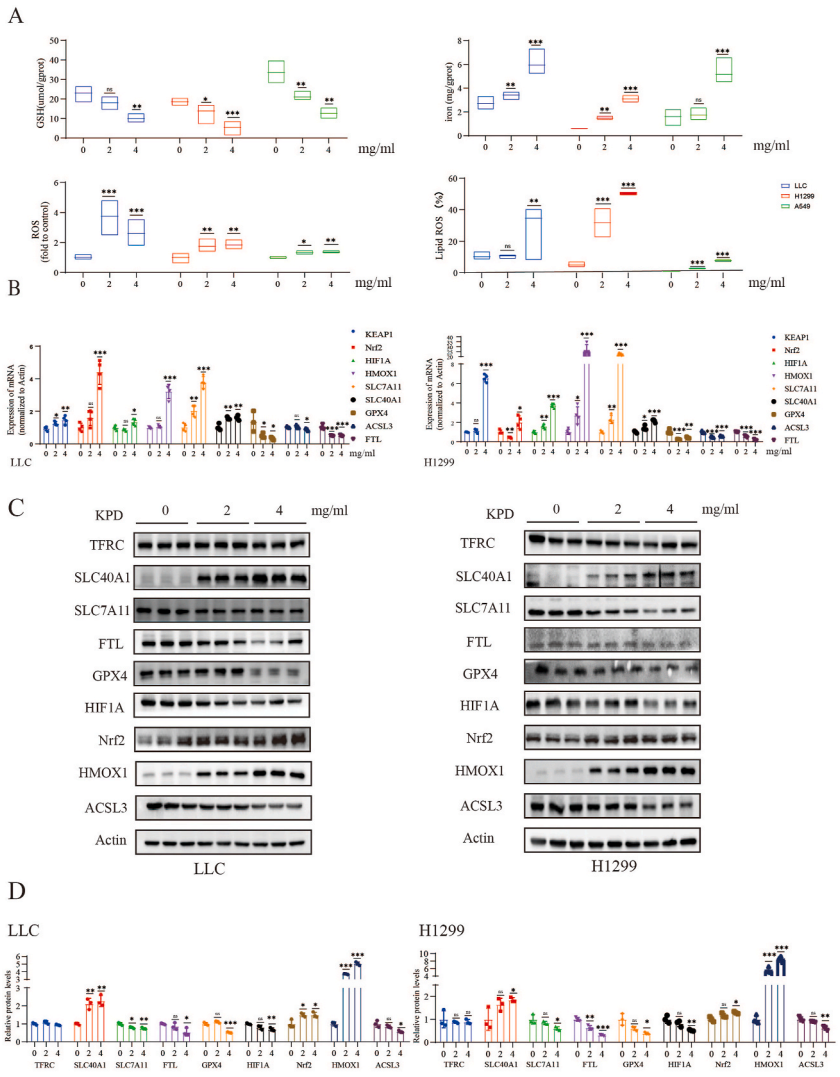

Fig. 3. STD induced ferroptosis in NSCLC cells. (A) The intracellular GSH, iron, ROS, and lipid ROS levels after STD treatment for 24 h in LLC and H1299 cells. (B) The expression of several key ferroptosis regulators was examined by RT-qPCR in NSCLC cells. (C–D) The expression of several key ferroptosis regulators, such as TFRC, SLC40A1, SLC7A11, FTL, GPX4, HIF1A, Nrf2, HMOX1, ACSL3 and Actin, was examined by WB in LLC and H1299 cells.

3. Results

3.1. STD shows a potential anti-lung cancer effect

Different doses of STD were administered to LLC, H1299, and A549 cell lines over various time periods to evaluate their cytotoxicity and inhibitory effects. Initially, cell viability was assessed using the CCK-8 assay. The results indicated that STD inhibited the proliferation of NSCLC cells, with nearly complete cell death observed at a concentration of 6 mg/ml of STD after 72 h (Fig. 1A). Subsequently, the EdU assay was employed to further investigate the effects of STD on cell proliferation. The results demonstrated that the STD-treated group exhibited a significantly lower number of EdU^+ cells compared to the control group (Fig. 1B), a finding that was corroborated by the colony formation assay (Fig. 1C). Cancer cell migration is a primary contributor to poor clinical outcomes. To assess the impact of STD on tumor cell migration, a wound-healing assay was conducted. The results revealed that STD effectively inhibited migration in both H1299 and A549 cells (Fig. 1D and Supplementary Fig. 1A). These data suggest a potential anti-tumor effect of STD on NSCLC cells.

3.2. Network pharmacology predicted ferroptosis as the main mechanism in STD-mediated NSCLC cell death

LC-MS analysis was conducted on STD to investigate the potential mechanisms underlying STD-mediated tumor cell killing. The results indicated that flavonoids, carboxylic acids, and their derivatives predominantly account for the compound's composition (Fig. 2A). Subsequently, we statistically identified the top 15 monomer components, as shown in Fig. 2B. Network pharmacology was then employed to elucidate the mechanisms associated with STD based on these components. A total of 17,991 lung cancer-related genes were retrieved from various databases, including 16 genes from the DrugBank database, 163 from the TTD database, 296 from the PharmGkb database, 170 from the OMIM database, and 17,944 from the GeneCards database (Fig. 2C). The TCMSP database was utilized to identify 163 target genes of STD. By taking the intersection of these datasets, we identified a total of 143 genes as potential therapeutic targets of STD for lung cancer (Fig. 2D). GO analysis revealed that these genes were primarily enriched for cellular responses to oxidative stress, ROS, and metal ions, all of which are implicated in ferroptosis (Fig. 2E). We speculated that STD might inhibit the progression of NSCLC by inducing ferroptosis. To further validate this hypothesis, we employed several inhibitors in our culture system, including Liproxstatin-1 (a ferroptosis inhibitor), chloroquine (an autophagy inhibitor), necrostatin-1 (a necroptosis inhibitor), and Z-VAD-FMK (a caspase inhibitor). Our results demonstrated that only Liproxstatin-1 significantly reversed STD-induced cell death in LLC, H1299, and A549 cells (Fig. 2F and G, Supplementary Fig. 1B), suggesting that ferroptosis, rather than other forms of cell death, is primarily responsible for STD-induced cell death. Additionally, the expression of GPX4 at the protein level supports this conclusion (Fig. 2H, Supplementary Fig. 1C).

3.3. STD induces ferroptosis in NSCLC cells in vitro

Ferroptosis is characterized by elevated iron accumulation, ROS, and lipid peroxidation, alongside reduced levels of GSH and GPX4 [4,30]. In light of this, we investigated the associated parameters in NSCLC cells following standard treatment (STD). Upon administration of STD, a ferroptosis morphology characterized by large membrane blebs, akin to that observed after treatment with RSL3, was noted in H1299 cells (Supplementary Fig. 1D). Our data indicated that STD-treated cells exhibited significantly higher levels of iron, ROS, and lipid peroxidation, coupled with significantly lower levels of GSH compared to control samples (Fig. 3A, Supplementary Fig. 2A). These findings suggest that STD can disrupt oxidative stress levels and iron homeostasis in NSCLC cells. Subsequently, we measured the mRNA expression levels of ferroptosis-related genes. In STD-treated LLC and H1299 cells, pro-ferroptosis genes such as Keap1, Nrf2, and HMOX1 were significantly upregulated, while anti-ferroptosis genes like GPX4, ACSL3, and FTL were downregulated compared to control samples. Notably, HIF1A, SLC7A11, and SLC40A1 were also enhanced (Fig. 3B). In A549 cells, some markers exhibited an inverted expression pattern. The mRNA levels of Keap1, Nrf2, HIF1A, HMOX1, SLC40A1, GPX4, and FTL were similar to those in the previous two cell lines; however, STD resulted in downregulation of SLC7A11 and upregulation of ACSL3 at the mRNA level (Supplementary Fig. 2B). Subsequently, we assessed protein levels using Western blot analysis. The results indicated that STD upregulated the expression of Nrf2 and HMOX1, while downregulating the expression of FTL, GPX4, HIF1A, and ACSL3 in LLC, H1299, and A549 cells, respectively. Notably, STD did not have a significant effect on the expression level of the TFRC protein (Fig. 3C and D, Supplementary Figs. 2C–D). Additionally, SLC40A1 levels were elevated, whereas SLC7A11 levels were decreased in both LLC and H1299 cells (Fig. 3C-D). However, these two protein levels did not exhibit significant changes following STD treatment in the A549 cell line (Supplementary Figs. 2C–D). Collectively, these results strongly suggest that STD primarily induces ferroptosis to eliminate NSCLC cells in *in vitro* trials. Numerous studies have established a link between the induction of ferroptosis and the activation of the Nrf2/HMOX1 pathway. The activity of HMOX1 catalyzes the oxidative cleavage of heme at the α-methene bridge carbon, generating equivalent amounts of CO and BV, while releasing the central heme iron chelate as Fe^{2+} [16]. Therefore, we hypothesize that the Nrf2/HMOX1 pathway plays a crucial role in regulating intracellular iron levels, as evidenced by the compensatory increases in SLC7A11 and SLC40A1.

Furthermore, overexpressed HMOX1 demonstrates antitumor activity in various malignancies [31,32]. The endoplasmic reticulum (ER) serves as the primary localization site for HMOX1, where it co-localizes with cytochrome P-450 reductase [33,34]. The immunofluorescence assay results indicated a significant increase in HMOX1 protein expression, which co-localized with the ER in LLC, H1299, and A549 cells after STD administration (Supplementary Fig. 3). These findings suggest that STD may elevate iron levels primarily through the enzymatic functions of HMOX1.

3.4. Knockdown of HMOX1 decreased STD-induced NSCLC cells ferroptosis

To verify this conjecture, we knocked down the expression of the HMOX1 gene in H1299 and A549 cells through the transfection of siRNA targeting HMOX1. The three siRNA candidates for HMOX1 demonstrated varying degrees of efficacy in reducing gene expression at the mRNA level, with siHMOX1-587 exhibiting the highest efficiency in inhibiting HO-1 expression compared to the other candidates. Consequently, siHMOX1-587 was selected for further experiments in this study (Fig. 4A and B). Functionally, the siRNA-mediated reduction of HMOX1 significantly mitigated the cytotoxic effects of STD on tumor cells (Fig. 4C). Furthermore, the knockdown of the HMOX1 gene led to a diminished increase in intracellular iron levels and a reduced depletion of GSH content in STD-treated tumor cells, relative to the STD-only treatment group (Fig. 4D and E). At the protein level, we also observed that the reduction in GPX4 and the upregulation of HMOX1 induced by STD was partially reversed by the knockdown of HMOX1 (Fig. 4F). These results elucidate the important role played by HMOX1 in STD-induced ferroptosis.

3.5. STD exerts antitumor efficacy by inducing ferroptosis in vivo

To elucidate the role of STD *in vivo*, we utilized a subcutaneous xenograft tumor model to evaluate the therapeutic potential of STD. Following the subcutaneous injection of LLC cells, C57BL/6J mice were randomly assigned to three experimental groups: the control group (CT), the low-dose STD group (512.5 mg/kg), and the high-dose STD group (1537.5 mg/kg) (Fig. 5A). No significant differences in body weight were observed among these experimental groups (Fig. 5B). Notably, STD therapy significantly inhibited tumor growth in the high-dose STD group compared to the control group (Fig. 5C). The levels of iron in both blood and tumor tissue exhibited a dose-dependent increase (Fig. 5D). To further investigate whether *in vivo* administration of STD induced ferroptosis, we assessed several ferroptosis-related markers in tumors using Western blot analysis. The data indicated that STD downregulated the expression of anti-ferroptosis proteins, including SLC7A11, FTL, GPX4, HIF1A, and ACSL3, while upregulating pro-ferroptosis proteins such as Nrf2 and HMOX1 (Fig. 5E). Additionally, a compensatory increase in SLC40A1 was observed, with no significant changes in the expression of TFRC (Fig. 5E). Furthermore, STD administration enhanced the expression of HMOX1 in tumor tissue, as demonstrated by

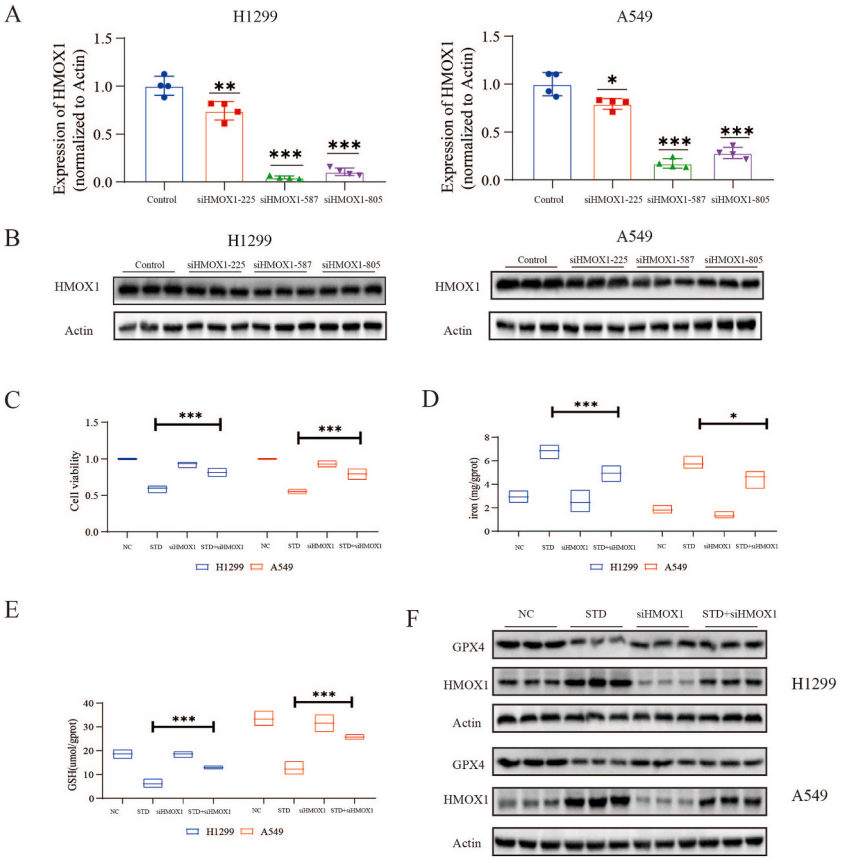

Fig. 4. Knockdown of HMOX1 reduced ferroptosis in NSCLC cells induced by STD. (A–B) The expression levels of HMOX1 were assessed using RT-qPCR and Western blotting in NSCLC cells transfected with siRNA targeting the human HMOX1 gene. (C–E) The cell viability, intracellular iron levels, and GSH levels of NSCLC cells were evaluated following treatment under the specified conditions. (F) The expression of the GPX4 and HMOX1 protein was also examined.

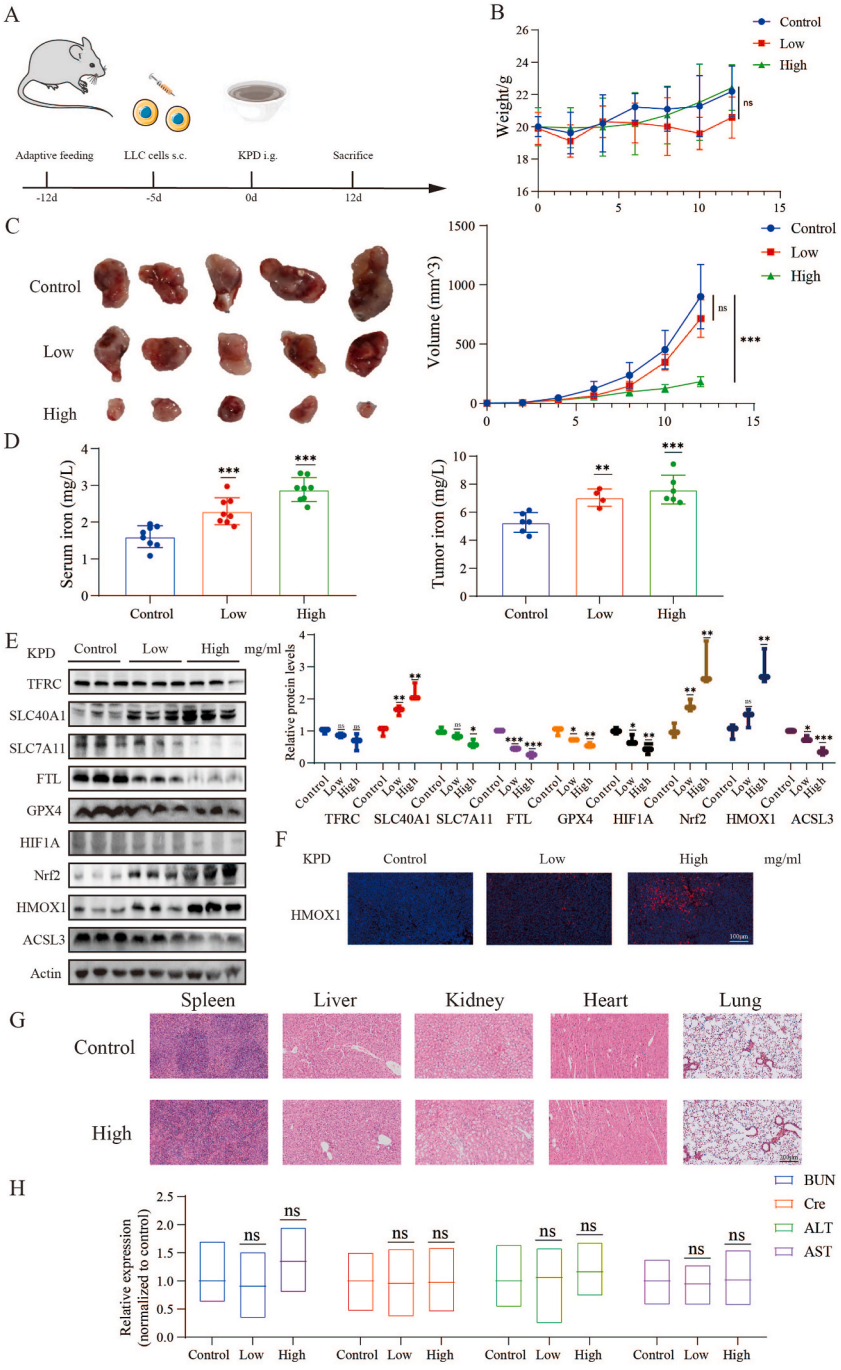

Fig. 5. STD suppresses tumor progression by ferroptosis *in vivo*. (A) C57BL/6J mice that carried tumor derived from LLC cells subcutaneous xenografts tumor were administered with STD (low dose: 512.5 mg/kg or high dose: 1537.5 mg/kg) or PBS every other day. (B) Body weights of the C57BL/6J mice during the experimental period. (C) Size of the subcutaneous tumor of xenografts in different groups of C57BL/6J mice. (D) The level of iron was detected in serum and tumor tissue. (E) The protein expression of ferroptosis-related markers was examined by WB. (F) Immunofluorescence results showed significantly higher levels of HMOX1 protein in tumor tissue in the STD therapy group. (G) H&E staining of major organs after 12 days of STD administration. Scale bar: 200 μm. (F) Serum BUN, Cre, ALT and AST levels after 12 days of STD administration.

immunofluorescence staining (Fig. 5F). To evaluate the side effects of STD in an *in vivo* model, various organs from the three groups were collected and stained with H&E. No histological differences were observed in the heart, liver, spleen, lung, or kidney (Fig. 5G). Subsequently, we performed blood examinations to assess liver and kidney functionality. The levels of aspartate aminotransferase (AST), alanine aminotransferase (ALT), creatinine (Cre), and blood urea nitrogen (BUN) showed no significant variations among the

three groups (Fig. 5H). This finding indicates that STD exhibited no observable toxicity in mice. Furthermore, these results demonstrate that STD prevents lung cancer development by inducing ferroptosis, thereby corroborating our *in vitro* cellular experiments.

3.6. STD alters TIME to induce antitumor immunity

Recent research has demonstrated that the tumor immune microenvironment (TIME) plays a crucial role in cancer development and influences clinical outcomes for individuals [35]. Therefore, we investigated the impact of standard treatment (STD) on antitumor

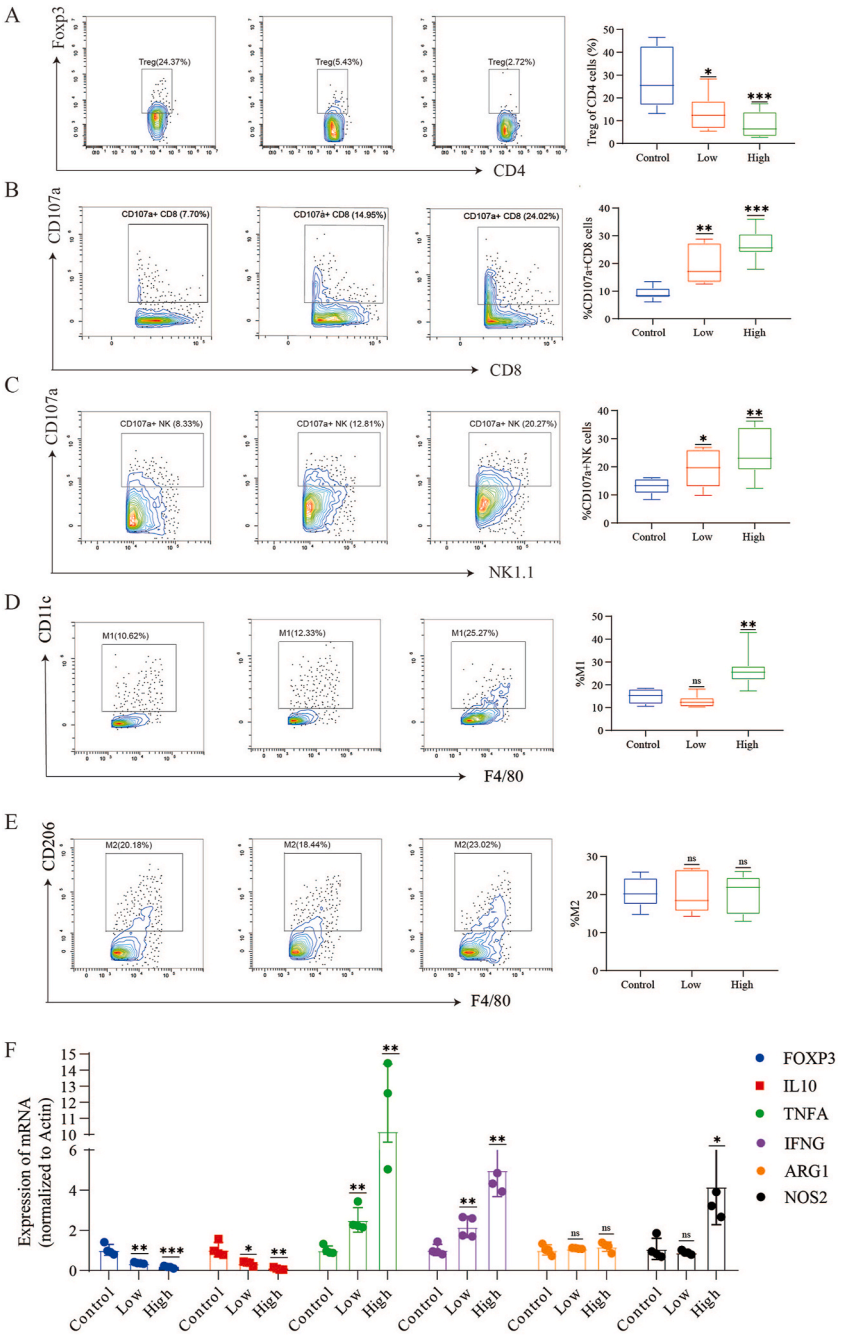

Fig. 6. Representative flow cytometry results of Treg, CD8, NK, M1 and M2 cells in TIME of subcutaneous xenografts tumor. (A) Flow cytometry to identify Treg cell populations in TIME. (B). Flow cytometry to identify CD107a^{+} CD8 cell populations in TIME. (C) Flow cytometry to identify CD107a^{+} NK cell populations in TIME. (D) Flow cytometry to identify M1 cell populations in TIME. (E) Flow cytometry to identify M2 cell populations in TIME. (F) The expression of several key TIME regulators was examined by RT-qPCR in tumor issues.

immunity using the C57BL/6J subcutaneous xenograft tumor model. The results revealed a decrease in the proportion of regulatory T (Treg) cells within the TIME following STD treatment (Fig. 6A). CD107a serves as a marker for degranulation and cytotoxic activity in $CD8^+$ T and natural killer (NK) cells [36]. Both low- and high-dose groups exhibited an increase in $CD107a^+$ CD8 cells and $CD107a^+$ NK cells within the tumors (Fig. 6B and C). M1 macrophages are known to limit tumor growth, while M2 macrophages promote tumor growth, angiogenesis, metastasis, and resistance to existing therapies [37]. Our data indicated that M1 macrophage levels were elevated only in the TIME of the high-dose STD-treated group (Fig. 6D), whereas no significant changes were observed in M2 macrophages (Fig. 6E). Next, we measured the mRNA levels of genes associated with TIME. The results showed that cytotoxicity-related genes, such as TNFA and IFNG, as well as the M1 marker gene NOS2, were significantly increased, while Treg cell marker genes, including FOXP3 and IL10, were decreased. No substantial changes were detected in the M2 cell marker gene Arg1 (Fig. 6F). Furthermore, we also investigated immune cells in the spleen. The absolute numbers of Treg, Th1, and Th17 cells were significantly higher in the STD therapy group in a dose-dependent manner (Supplementary Figs. 4A–C). Similar to the findings in the TIME, the expression of M1 macrophages in the STD treatment group was higher than that in the control group (Supplementary Fig. 4D). However, M2 macrophages in the high-dose group exhibited a trend toward significant reduction (Supplementary Fig. 4E). These data suggest that STD treatment can reshape the TIME, which may represent another aspect of its antitumor effect *in vivo*.

3.7. The expression pattern of ferroptosis-related genes were identical in human LUAD

We screened nine proteins associated with ferroptosis. To determine whether a similar trend exists in clinical tumor samples, we conducted a bioinformatics analysis of their potential associations with clinical outcomes using the Cancer Genome Atlas (TCGA) database. The expression levels of genes such as TFRC, SLC40A1, HMOX1, FTL, and Nrf2 were found to be reduced in the LUAD tumor group compared to the normal group (Fig. 7A). Conversely, the mRNA expression of HIF1A, SLC7A11, GPX4, and ACSL3 was upregulated in the LUAD tumor group (Fig. 7B). Comparable results were observed in the paired analysis of normal and tumor tissues from the same patient, with the exception of GPX4, which showed no significant trend (Fig. 7C and D). Survival analysis indicated that LUAD patients with high expression levels of FTL, SLC40A1, GPX4, and Nrf2 had longer survival compared to those with low expression levels (Supplementary Fig. 5A). In contrast, high levels of HIF1A, SLC7A11, and ACSL3 expression were associated with a shorter lifespan for LUAD patients (Supplementary Fig. 5B). The expression of HMOX1 and TFRC did not appear to affect the survival

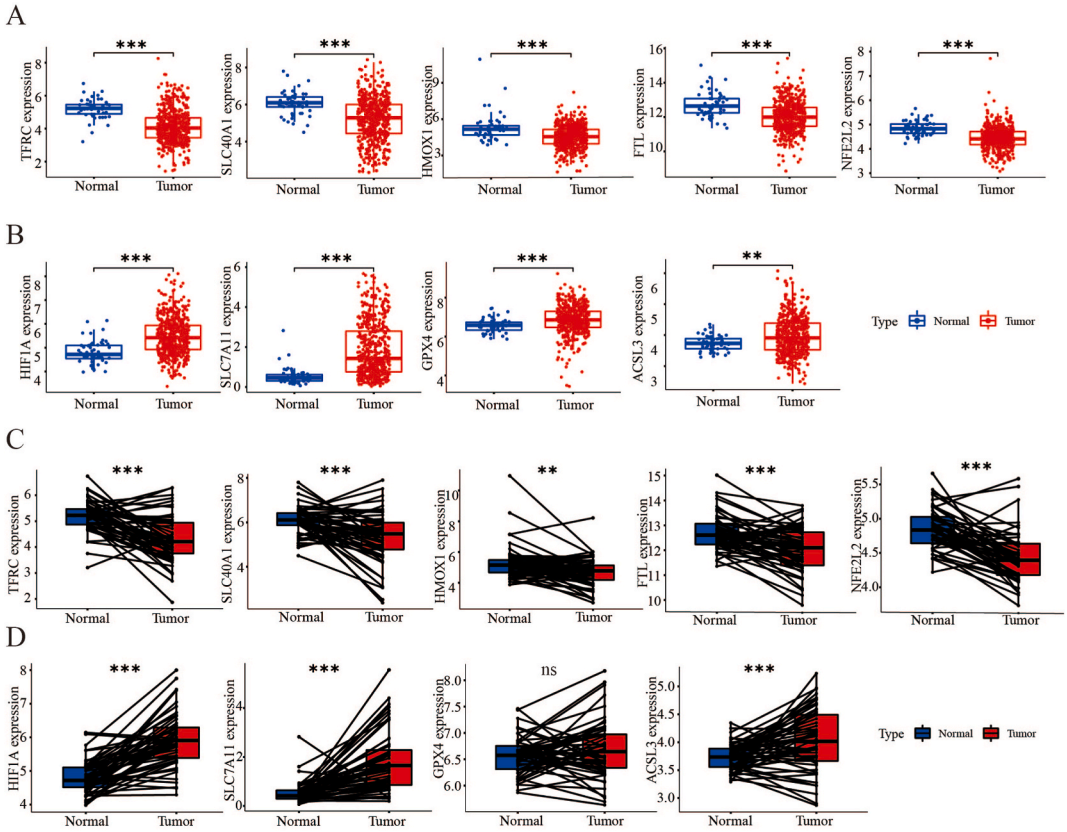

Fig. 7. Discrepant expression of ferroptosis-related genes in the normal and tumor samples. (A–B) Differential expression of ferroptosis-related genes between normal and tumor samples by Wilcoxon rank sum test. (C–D) Ferroptosis-related genes was compared in normal and tumor samples derived from the same patient using paired differentiation analysis by Wilcoxon rank sum test.

time of LUAD patients (Supplementary Fig. 5C). These analyses suggest that ferroptosis-related genes may serve as prognostic markers in human LUAD.

4. Discussion

TCM has garnered global attention for its effectiveness in treating and preventing cancer [38]. STD, a compound originated from Chinese medicine with *Sophora alopecuroides* and *Taraxacum*, is widely utilized in treating cancer. However, the underlying mechanism remains largely unknown. In the current study, ex vivo tests were used to first determine the anticancer effects of STD in NCSLC. The anti-tumor effect of STD via inducing ferroptosis was then revealed. Additionally, we identified the increased HMOX1 protein expression and its enzymatic activity, which may be the cause of ferroptosis. We then discovered that STD can change the TIME to exert antitumor effects. Finally, bioinformatics analysis revealed a strong association between lung cancer patient prognosis and ferroptosis-related genes impacted by STD.

The primary objective of traditional cancer treatment is to induce apoptosis in cancer cells; however, many cancer cells exhibit either resistance to chemotherapy or a deficiency in apoptosis. Consequently, it is essential to explore novel medications or therapies that can induce non-apoptotic cell death, providing cancer patients with a promising new treatment avenue. Ferroptosis, an iron-dependent form of cell death, differs from apoptosis in terms of morphology, biochemistry, and genetics [4,39]. There is growing interest in drugs that induce ferroptosis, which may lead to the development of innovative cancer treatment strategies [15,40]. One of the defining features of ferroptosis is the accumulation of Fe^{2+} and lipid ROS, both of which are critical determinants of cell fate [41]. Cellular iron metabolism encompasses three primary processes: iron uptake, storage, and export [42]. TFRC is a membrane protein that facilitates iron uptake, while FTH and FTL serve as the principal intracellular iron storage proteins [43]. Further, SLC40A1 mediates iron export in tumor cells [44]. Heme was dissolved into Fe^{2+}, carbon monoxide and biliverdin by HMOX1 protein [45]. And Nrf2 serves as an important regulator of HMOX1. GPX4, SLC7A11 and HIF1A have a strong connection with ROS. Moreover, mono-unsaturated fatty acids, such as oleic acid, require ACSL3 in order to exert anti-ferroptosis effects [46]. Until now, agents based on metal irons have been in the early stages of development. More extensive studies and even clinical trials are needed to confirm their efficacy [47]. Our findings revealed that ferroptosis may serve as the main pathway because ferroptosis inhibitor Fer-1 reversed STD-induced cell death. Additionally, STD therapy significantly induced ROS and iron accumulation, GSH depletion, and lipid peroxidation. In the following study, elevated SLC40A1 transferrin was found, indicating that iron was kept at a high level in lung cancer cells, which might be due to increased HO-1-mediated iron upregulation. In addition, the reduced FTL also indicated a weakened intracellular iron storage capacity. The reduced GPX4 and SLC7A11 surface a weakened antioxidant reducing capacity of the tumor under the intervention of STD.

Therapeutic resistance remains a major challenge in clinic. How tumor cells respond to therapy is not solely dependent on the genomic aberrations they harbor but also is regulated by the TIME, mainly involving tumor cells and infiltrating immune cells including tumor-associated macrophages, B cells, NK cells, and T cells [48]. In recent years, the anti-tumor effects of herbal compounding in modulating TIME have also been widely reported. Here, we showed that STD inhibited the progression of subcutaneous xenograft tumors without apparent toxicity in *in vivo* model. Alterations of the pro-ferroptosis proteins (TFRC, FTL, Nrf2 and HMOX1) and ferroptosis suppressor proteins (SLC40A1, SLC7A11, GPX4, HIF1A and ACSL3) were detected in tumors after STD therapy. Furthermore, we also found that the administration of STD reduced the percentage of Treg cells in TIME. And we observed that $CD107a^+$ CD8 and $CD107a^+$ NK cells were also increased in a dose-dependent. M1 macrophages, widely considered to exert anti-tumor effect, was increased in the high-dose group. In addition, STD alters the proportion of immune cells in the spleen. To sum up, STD owns an effect on reshaping TIME towards tumor suppression. Nevertheless, the direct relationship between STD-induced ferroptosis in NSCLC and changes in the TIME requires further investigation.

5. Conclusion

In summary, our data provided compelling evidence demonstrating that STD promotes NSCLC ferroptosis, accompanied by cell cycle arrest, inhibition of cell proliferation and migration. In addition, high therapeutic efficacy, low toxicity, and high selectivity shown in *in vivo* mouse models prove that STD serves as a potential decoction for NSCLC therapy. However, the specific mechanism of STD-induced ferroptosis and its possible target proteins still need to be further explored.

CRediT authorship contribution statement

Ouyang Xiaohu: Formal analysis, Data curation, Conceptualization. **Jingbo Wang:** Formal analysis, Data curation, Conceptualization. **Xiaoyuan Qiu:** Methodology, Investigation, Formal analysis. **Shuxin Song:** Investigation, Funding acquisition, Conceptualization. **Junyi Li:** Methodology, Investigation, Formal analysis. **Shanshan Luo:** Investigation, Funding acquisition, Formal analysis. **Qianyun Chen:** Investigation, Funding acquisition, Data curation. **Desheng Hu:** Investigation, Funding acquisition, Formal analysis, Data curation, Conceptualization.

Ethics approval and consent to participate

Our study was performed according to the international, national and institutional rules considering animal experiments. The protocol for using animals was approved by Ethics Review Committee for Animal Experimentation of Huazhong University of Science

and Technology. The Ethical Inspection Number:[2023]IACUC: 3554.

Data availability

RNA sequencing data used in this study is available at https://portal.gdc.cancer.gov/. The potential targets of STD are available at https://old.tcmsp-e.com/tcmsp. And the targets of NSCLC are available in https://www.genecards.org/, https://www.omim.org/, https://www.pharmgkb.org/, https://db.idrblab.net/ttd/, and https://go.drugbank.com/.

Consent for publication

The authors declare that they consent to publish this manuscript.

Funding

This work has been financially supported by the National Natural Science Foundation of China (Nos. 82274317, 81974249, 82070136, 82104488).

Declaration of competing interest

The authors declare that they have no known competing financial interests or personal relationships that could have appeared to influence the work reported in this paper.

Acknowledgements

Not applicable.

Appendix A. Supplementary data

Supplementary data to this article can be found online at https://doi.org/10.1016/j.heliyon.2024.e39564.

References

[1] H. Sung, J. Ferlay, R.L. Siegel, M. Laversanne, I. Soerjomataram, A. Jemal, F. Bray, Global cancer statistics 2020: GLOBOCAN estimates of incidence and mortality worldwide for 36 cancers in 185 countries, CA A Cancer J. Clin. 71 (2021) 209–249, https://doi.org/10.3322/caac.21660.
[2] R.L. Siegel, K.D. Miller, N.S. Wagle, A. Jemal, Cancer statistics, 2023, CA A Cancer J. Clin. 73 (2023) 17–48, https://doi.org/10.3322/caac.21763.
[3] J.X. Li, R.Z. Li, A. Sun, H. Zhou, E. Neher, J.S. Yang, J.M. Huang, Y.Z. Zhang, Z.B. Jiang, T.L. Liang, et al., Metabolomics and integrated network pharmacology analysis reveal Tricin as the active anti-cancer component of Weijing decoction by suppression of PRKCA and sphingolipid signaling, Pharmacol. Res. 171 (2021) 105574, https://doi.org/10.1016/j.phrs.2021.105574.
[4] S.J. Dixon, K.M. Lemberg, M.R. Lamprecht, R. Skouta, E.M. Zaitsev, C.E. Gleason, D.N. Patel, A.J. Bauer, A.M. Cantley, W.S. Yang, et al., Ferroptosis: an iron-dependent form of nonapoptotic cell death, Cell 149 (2012) 1060–1072, https://doi.org/10.1016/j.cell.2012.03.042.
[5] K. Kajiwara, O. Beharier, C.P. Chng, J.P. Goff, Y. Ouyang, C.M. St Croix, C. Huang, V.E. Kagan, K.J. Hsia, Y. Sadovsky, Ferroptosis induces membrane blebbing in placental trophoblasts, J. Cell Sci. 135 (2022), https://doi.org/10.1242/jcs.255737.
[6] X. Chen, R. Kang, G. Kroemer, D. Tang, Broadening horizons: the role of ferroptosis in cancer, Nat. Rev. Clin. Oncol. 18 (2021) 280–296, https://doi.org/10.1038/s41571-020-00462-0.
[7] N. Geng, B.J. Shi, S.L. Li, Z.Y. Zhong, Y.C. Li, W.L. Xua, H. Zhou, J.H. Cai, Knockdown of ferroportin accelerates erastin-induced ferroptosis in neuroblastoma cells, Eur. Rev. Med. Pharmacol. Sci. 22 (2018) 3826–3836, https://doi.org/10.26355/eurrev_201806_15267.
[8] J. Zhao, Y. Chen, T. Xiong, S. Han, C. Li, Y. He, Y. He, G. Zhao, T. Wang, L. Wang, et al., Clustered cobalt nanodots initiate ferroptosis by upregulating heme oxygenase 1 for radiotherapy sensitization, Small 19 (2023) e2206415, https://doi.org/10.1002/smll.202206415.
[9] H. Cheng, P. Wang, N. Wang, W. Dong, Z. Chen, M. Wu, Z. Wang, Z. Yu, D. Guan, L. Wang, et al., Neuroprotection of NRF2 against ferroptosis after traumatic brain injury in mice, Antioxidants 12 (2023), https://doi.org/10.3390/antiox12030731.
[10] X. Yang, Y. Chen, W. Song, T. Huang, Y. Wang, Z. Chen, F. Chen, Y. Liu, X. Wang, Y. Jiang, et al., Review of the role of ferroptosis in testicular function, Nutrients 14 (2022), https://doi.org/10.3390/nu14245268.
[11] S. Zheng, X.Y. Guan, Ferroptosis: promising approach for cancer and cancer immunotherapy, Cancer Lett. 561 (2023) 216152, https://doi.org/10.1016/j.canlet.2023.216152.
[12] Y. Yang, T. Zhu, X. Wang, F. Xiong, Z. Hu, X. Qiao, X. Yuan, D. Wang, ACSL3 and ACSL4, distinct roles in ferroptosis and cancers, Cancers 14 (2022), https://doi.org/10.3390/cancers14235896.
[13] D. Zhang, D. Man, J. Lu, Y. Jiang, B. Ding, R. Su, R. Tong, J. Chen, B. Yang, S. Zheng, et al., Mitochondrial TSPO promotes hepatocellular carcinoma progression through ferroptosis inhibition and immune evasion, Adv. Sci. (2023) e2206669, https://doi.org/10.1002/advs.202206669.
[14] Z. Zhang, H. Zhu, C. Zhao, D. Liu, J. Luo, Y. Ying, Y. Zhong, DDIT4 promotes malignancy of head and neck squamous cell carcinoma, Mol. Carcinog. 62 (2023) 332–347, https://doi.org/10.1002/mc.23489.
[15] C. Zhou, T. Yu, R. Zhu, J. Lu, X. Ouyang, Z. Zhang, Q. Chen, J. Li, J. Cui, F. Jiang, et al., Timosaponin AIII promotes non-small-cell lung cancer ferroptosis through targeting and facilitating HSP90 mediated GPX4 ubiquitination and degradation, Int. J. Biol. Sci. 19 (2023) 1471–1489, https://doi.org/10.7150/ijbs.77979.
[16] R. Tenhunen, H.S. Marver, R. Schmid, Microsomal heme oxygenase. Characterization of the enzyme, J. Biol. Chem. 244 (1969) 6388–6394.
[17] J.A. Choi, E.H. Lee, H. Cho, J.H. Kim, High-dose selenium induces ferroptotic cell death in ovarian cancer, Int. J. Mol. Sci. 24 (2023), https://doi.org/10.3390/ijms24031918.

[18] B. Hassannia, P. Vandenabeele, T. Vanden Berghe, Targeting ferroptosis to iron out cancer, Cancer Cell 35 (2019) 830–849, https://doi.org/10.1016/j.ccell.2019.04.002.
[19] S.C. Koeberle, A.P. Kipp, H. Stuppner, A. Koeberle, Ferroptosis-modulating small molecules for targeting drug-resistant cancer: challenges and opportunities in manipulating redox signaling, Med. Res. Rev. (2023), https://doi.org/10.1002/med.21933.
[20] Y.Y. Zhao, Y.Q. Yang, H.H. Sheng, Q. Tang, L. Han, S.M. Wang, W.Y. Wu, GPX4 plays a crucial role in Fuzheng Kang'ai decoction-induced non-small cell lung cancer cell ferroptosis, Front. Pharmacol. 13 (2022) 851680, https://doi.org/10.3389/fphar.2022.851680.
[21] Y. Huang, P. Xiang, Y. Chen, Q. Pan, K. Yuan, Alantolactone facilitates ferroptosis in non-small cell lung cancer through promoting FTH1 ubiquitination and degradation, Chem. Biol. Drug Des. 104 (2024) e14560, https://doi.org/10.1111/cbdd.14560.
[22] X. Zhang, W. Cai, Y. Yan, Agrimonolide inhibits the malignant progression of non-small cell lung cancer and induces ferroptosis through the mTOR signaling pathway, Anti Cancer Agents Med. Chem. (2024), https://doi.org/10.2174/0118715206305421240715042502.
[23] X. Wang, T. Zhang, L. Qu, Y. Zhang, G. Gao, Auriculasin induces mitochondrial oxidative stress and drives ferroptosis by inhibiting PI3K/Akt pathway in non-small cell lung cancer, Naunyn-Schmiedeberg's Arch. Pharmacol. (2024), https://doi.org/10.1007/s00210-024-03328-9.
[24] B. Zhao, X. Hui, L. Jiao, L. Bi, L. Wang, P. Huang, W. Yang, Y. Yin, S. Jin, C. Wang, et al., A TCM formula YYWY inhibits tumor growth in non-small cell lung cancer and enhances immune-response through facilitating the maturation of dendritic cells, Front. Pharmacol. 11 (2020) 798, https://doi.org/10.3389/fphar.2020.00798.
[25] L. Wang, W. Wu, X. Zhu, W. Ng, C. Gong, C. Yao, Z. Ni, X. Yan, C. Fang, S. Zhu, The ancient Chinese decoction Yu-Ping-Feng suppresses orthotopic Lewis lung cancer tumor growth through increasing M1 macrophage polarization and CD4(+) T cell cytotoxicity, Front. Pharmacol. 10 (2019) 1333, https://doi.org/10.3389/fphar.2019.01333.
[26] L. Kang, M.S. Miao, Y.G. Song, X.Y. Fang, J. Zhang, Y.N. Zhang, J.X. Miao, Total flavonoids of Taraxacum mongolicum inhibit non-small cell lung cancer by regulating immune function, J. Ethnopharmacol. 281 (2021) 114514, https://doi.org/10.1016/j.jep.2021.114514.
[27] J. Lu, B. Shuai, Z. Shou, W. Guo, C. Zhou, X. Ouyang, H. Zhou, J. Li, J. Cui, F. Jiang, et al., Taraxasterol inhibits tumor growth by inducing apoptosis and modulating the tumor microenvironment in non-small cell lung cancer, Cancers 14 (2022), https://doi.org/10.3390/cancers14194645.
[28] S. Chen, S. Ma, H. Wang, X. Shao, B. Ding, Z. Guo, X. Chen, Y. Wang, Unraveling the mechanism of alkaloids from Sophora alopecuroides Linn combined with immune checkpoint blockade in the treatment of non-small cell lung cancer based on systems pharmacology, Bioorg. Med. Chem. 64 (2022) 116724, https://doi.org/10.1016/j.bmc.2022.116724.
[29] Y. Hou, H. Liang, E. Rao, W. Zheng, X. Huang, L. Deng, Y. Zhang, X. Yu, M. Xu, H. Mauceri, et al., Non-canonical NF-kappaB antagonizes STING sensor-mediated DNA sensing in radiotherapy, Immunity 49 (2018) 490–503 e494, https://doi.org/10.1016/j.immuni.2018.07.008.
[30] F. He, P. Zhang, J. Liu, R. Wang, R.J. Kaufman, B.C. Yaden, M. Karin, ATF4 suppresses hepatocarcinogenesis by inducing SLC7A11 (xCT) to block stress-related ferroptosis, J. Hepatol. (2023), https://doi.org/10.1016/j.jhep.2023.03.016.
[31] J.C. Becker, H. Fukui, Y. Imai, A. Sekikawa, T. Kimura, H. Yamagishi, N. Yoshitake, T. Pohle, W. Domschke, T. Fujimori, Colonic expression of heme oxygenase-1 is associated with a better long-term survival in patients with colorectal cancer, Scand. J. Gastroenterol. 42 (2007) 852–858, https://doi.org/10.1080/00365520701192383.
[32] G. Li Volti, D. Tibullo, L. Vanella, C. Giallongo, F. Di Raimondo, S. Forte, M. Di Rosa, S.S. Signorelli, I. Barbagallo, The heme oxygenase system in hematological malignancies, Antioxidants Redox Signal. 27 (2017) 363–377, https://doi.org/10.1089/ars.2016.6735.
[33] W. Durante, Targeting heme oxygenase-1 in the arterial response to injury and disease, Antioxidants 9 (2020), https://doi.org/10.3390/antiox9090829.
[34] W.J. Huber 3rd, W.L. Backes, Expression and characterization of full-length human heme oxygenase-1: the presence of intact membrane-binding region leads to increased binding affinity for NADPH cytochrome P450 reductase, Biochemistry 46 (2007) 12212–12219, https://doi.org/10.1021/bi701496z.
[35] J.U. Lim, E. Lee, S.Y. Lee, H.J. Cho, D.H. Ahn, Y. Hwang, J.Y. Choi, C.D. Yeo, C.K. Park, S.J. Kim, Current literature review on the tumor immune microenvironment, its heterogeneity and future perspectives in treatment of advanced non-small cell lung cancer, Transl. Lung Cancer Res. 12 (2023) 857–876, https://doi.org/10.21037/tlcr-22-633.
[36] E. Aktas, U.C. Kucuksezer, S. Bilgic, G. Erten, G. Deniz, Relationship between CD107a expression and cytotoxic activity, Cell. Immunol. 254 (2009) 149–154, https://doi.org/10.1016/j.cellimm.2008.08.007.
[37] Q. Zhang, M. Sioud, Tumor-associated macrophage subsets: shaping polarization and targeting, Int. J. Mol. Sci. 24 (2023), https://doi.org/10.3390/ijms24087493.
[38] Y. You, X. Chen, X. Chen, H. Li, R. Zhou, J. Zhou, M. Chen, B. Peng, S. Ji, H.Y. Kwan, et al., Jiawei Yanghe Decoction suppresses breast cancer by regulating immune responses via JAK2/STAT3 signaling pathway, J. Ethnopharmacol. (2023) 116358, https://doi.org/10.1016/j.jep.2023.116358.
[39] X. Ouyang, J. Zhou, L. Lin, Z. Zhang, S. Luo, D. Hu, Pyroptosis, inflammasome, and gasdermins in tumor immunity, Innate Immun. 29 (2023) 3–13, https://doi.org/10.1177/17534259221143216.
[40] X. Ouyang, R. Zhu, L. Lin, X. Wang, Q. Zhuang, D. Hu, GAPDH is a novel ferroptosis-related marker and correlates with immune microenvironment in lung adenocarcinoma, Metabolites 13 (2023), https://doi.org/10.3390/metabo13020142.
[41] F. Zheng, Y. Wang, Q. Zhang, Q. Chen, C.L. Liang, H. Liu, F. Qiu, Y. Chen, H. Huang, W. Lu, et al., Polyphyllin I suppresses the gastric cancer growth by promoting cancer cell ferroptosis, Front. Pharmacol. 14 (2023) 1145407, https://doi.org/10.3389/fphar.2023.1145407.
[42] Y. Zhao, Z. Huang, H. Peng, Molecular mechanisms of ferroptosis and its roles in hematologic malignancies, Front. Oncol. 11 (2021) 743006, https://doi.org/10.3389/fonc.2021.743006.
[43] Y. Jin, L. Zhao, S. Wang, X. Zhang, J. Quan, Z. Lin, J. Piao, RSL1D1 knockdown induces ferroptosis and mediates ferrous iron accumulation in senescent cells by inhibiting FTH1 mRNA stability, Carcinogenesis (2023), https://doi.org/10.1093/carcin/bgad012.
[44] P. Xu, F.H. Ge, W.X. Li, Z. Xu, X.L. Wang, J.L. Shen, A.B. Xu, R.R. Hao, MicroRNA-147a targets SLC40A1 to induce ferroptosis in human glioblastoma, Anal. Cell Pathol. 2022 (2022) 2843990, https://doi.org/10.1155/2022/2843990.
[45] S. Ghareghomi, F. Moosavi-Movahedi, L. Saso, M. Habibi-Rezaei, A. Khatibi, J. Hong, A.A. Moosavi-Movahedi, Modulation of Nrf2/HO-1 by natural compounds in lung cancer, Antioxidants 12 (2023), https://doi.org/10.3390/antiox12030735.
[46] L. Magtanong, P.J. Ko, M. To, J.Y. Cao, G.C. Forcina, A. Tarangelo, C.C. Ward, K. Cho, G.J. Patti, D.K. Nomura, et al., Exogenous monounsaturated fatty acids promote a ferroptosis-resistant cell state, Cell Chem. Biol. 26 (2019) 420–432 e429, https://doi.org/10.1016/j.chembiol.2018.11.016.
[47] G. Manzari Tavakoli, M.H. Mirzapour, S. Razi, N. Rezaei, Targeting ferroptosis as a cell death pathway in Melanoma: from molecular mechanisms to skin cancer treatment, Int. Immunopharm. 119 (2023) 110215, https://doi.org/10.1016/j.intimp.2023.110215.
[48] T. Wu, Y. Dai, Tumor microenvironment and therapeutic response, Cancer Lett. 387 (2017) 61–68, https://doi.org/10.1016/j.canlet.2016.01.043.